cells

MDPI

Article

Multisystemic Cellular Tropism of SARS-CoV-2 in Autopsies of COVID-19 Patients

Dickson W. L. Wong [1,†], Barbara M. Klinkhammer [1,†], Sonja Djudjaj [1,†], Sophia Villwock [1], M. Cherelle Timm [1], Eva M. Buhl [1,2], Sophie Wucherpfennig [1], Claudio Cacchi [1], Till Braunschweig [1], Ruth Knüchel-Clarke [1], Danny Jonigk [3,4], Christopher Werlein [4], Roman D. Bülow [1], Edgar Dahl [1], Saskia von Stillfried [1,*] and Peter Boor [1,2,5,*]

1 Institute of Pathology, RWTH Aachen University Hospital, 52074 Aachen, Germany; dwong@ukaachen.de (D.W.L.W.); bklinkhammer@ukaachen.de (B.M.K.); sdjudjaj@ukaachen.de (S.D.); svillwock@ukaachen.de (S.V.); mtimm@ukaachen.de (M.C.T.); ebuhl@ukaachen.de (E.M.B.); swucherpfenn@ukaachen.de (S.W.); ccacchi@ukaachen.de (C.C.); tbraunschweig@ukaachen.de (T.B.); rknuechel-clarke@ukaachen.de (R.K.-C.); rbuelow@ukaachen.de (R.D.B.); edahl@ukaachen.de (E.D.)
2 Electron Microscopy Facility, RWTH Aachen University Hospital, 52074 Aachen, Germany
3 Institute of Pathology, Hannover Medical School, 30625 Hannover, Germany; jonigk.danny@mh-hannover.de
4 Member of the German Center for Lung Research (DZL), Biomedical Research in Endstage and Obstructive Lung Disease Hannover (BREATH), 30625 Hannover, Germany; Werlein.Christopher@mh-hannover.de
5 Department of Nephrology and Immunology, RWTH Aachen University Hospital, 52074 Aachen, Germany
* Correspondence: svonstillfri@ukaachen.de (S.v.S.); pboor@ukaachen.de (P.B.); Tel.: +49-241-80-85227 (P.B.); Fax: +49-241-80-82446 (P.B.)
† Equally contributed.

Citation: Wong, D.W.L.; Klinkhammer, B.M.; Djudjaj, S.; Villwock, S.; Timm, M.C.; Buhl, E.M.; Wucherpfennig, S.; Cacchi, C.; Braunschweig, T.; Knüchel-Clarke, R.; et al. Multisystemic Cellular Tropism of SARS-CoV-2 in Autopsies of COVID-19 Patients. *Cells* **2021**, *10*, 1900. https://doi.org/10.3390/cells10081900

Academic Editor: Ezequiel Álvarez

Received: 20 June 2021
Accepted: 22 July 2021
Published: 27 July 2021

Abstract: Multiorgan tropism of SARS-CoV-2 has previously been shown for several major organs. We have comprehensively analyzed 25 different formalin-fixed paraffin-embedded (FFPE) tissues/organs from autopsies of fatal COVID-19 cases (n = 8), using histopathological assessment, detection of SARS-CoV-2 RNA using polymerase chain reaction and RNA in situ hybridization, viral protein using immunohistochemistry, and virus particles using transmission electron microscopy. SARS-CoV-2 RNA was mainly localized in epithelial cells across all organs. Next to lung, trachea, kidney, heart, or liver, viral RNA was also found in tonsils, salivary glands, oropharynx, thyroid, adrenal gland, testicles, prostate, ovaries, small bowel, lymph nodes, skin and skeletal muscle. Viral RNA was predominantly found in cells expressing ACE2, TMPRSS2, or both. The SARS-CoV-2 replicating RNA was also detected in these organs. Immunohistochemistry and electron microscopy were not suitable for reliable and specific SARS-CoV-2 detection in autopsies. These findings were validated using in situ hybridization on external COVID-19 autopsy samples (n = 9). Apart from the lung, correlation of viral detection and histopathological assessment did not reveal any specific alterations that could be attributed to SARS-CoV-2. In summary, SARS-CoV-2 and its replication could be observed across all organ systems, which co-localizes with ACE2 and TMPRSS2 mainly in epithelial but also in mesenchymal and endothelial cells. Apart from the respiratory tract, no specific (histo-)morphologic alterations could be assigned to the SARS-CoV-2 infection.

Keywords: formalin-fixed paraffin-embedded (FFPE) tissue; post-mortem; histology; SARS-CoV-2; ACE2; TMPRSS2

1. Introduction

Since late 2019, the severe acute respiratory syndrome coronavirus 2 (SARS-CoV-2) causing the coronavirus disease 2019 (COVID-19) has caused a pandemic with major impacts on virtually all aspects of life. By July 2021, the number of global deaths attributed to COVID-19 has increased to more than 4 million, with more than 190 million infected individuals in 223 countries (WHO; https://covid19.who.int/ (accessed on 23 July 2021)). Despite extensive research, understanding of the organic and cellular manifestations of COVID-19

remains incomplete. Next to the typical clinical symptoms of respiratory infection [1], including fever, dyspnea, and dry cough, other symptoms indicate the involvement of other organ systems, e.g., diarrhea, vomiting, or anosmia. In severe cases, patients develop acute respiratory distress syndrome (ARDS), pneumonia but also systemic inflammation, heart diseases (e.g., elevated cardiac markers, acute heart failure) [2], and acute kidney injury (AKI). These data suggest that COVID-19 can be viewed as a multisystemic disease.

Endothelial dysfunction was proposed as an important factor in the pathogenesis of severe COVID-19. Endothelial cells express the receptors required for SARS-CoV-2 entry into the cells, i.e., angiotensin-converting enzyme 2 (ACE2) and transmembrane protease serine subtype 2 (TMPRSS2) [3]. Endothelial dysfunction (i.e., losing anti-coagulation and anti-fibrinolysis properties) has been shown to associate with thromboembolism during COVID-19. TMPRSS2 primes the viral spike protein together with ACE2, leading to the internalization of SARS-CoV-2 into the host cell [4]. This is followed by uncoating and the release of the genomic RNA, which is then used to synthesize polyproteins, i.e., pp1a and pp1abthat bind to the genomic RNA and trigger viral replication [5]. In clinical studies, ACE2 was found to be over-expressed in various tissues in patients, particularly with diabetes [6] or hypertension [7]. This might have implications for the higher incidence of COVID-19 in patients with these diseases.

Post-mortem investigation, i.e., autopsy, provides a comprehensive insight into the pathophysiology of novel diseases such as COVID-19, allowing investigation of the multisystemic viral spread and effects on a tissue and cellular level [8]. Recent studies using in situ hybridization (ISH) have found SARS-CoV-2 tropism and replication in airways, i.e., trachea, lung, bronchi, or submucosal glands, within pneumocytes, alveolar and pulmonary lymph node macrophages, endothelium, and respiratory epithelium [9–16]. In the extra-respiratory organs, ISH demonstrated direct infection of vascular endothelium in the kidney (renal proximal and distal tubular epithelial cells) [14,17–19], heart [15], liver [14], brain stem and leptomeninges [14] and placenta (syncytiotrophoblast and cytotrophoblast) [20]. However, the tissue and cellular association of SARS-CoV-2 genomic sense RNA and antisense RNA (indicating replication), ACE2 and TMPRSS2, across the various tissues were not comprehensively described [21]. Here, we used a multitude of different methods to analyze the distribution of SARS-CoV-2 virus, ACE2, and TMPRSS2 in 25 different organs, using formalin-fixed paraffin-embedded (FFPE) autopsy specimens from deceased COVID-19 patients.

2. Methods

2.1. Ethical Issues

The study was approved by the local ethics committee (EK 304/20, EK 119/20, EK 092/20 and 9621_BO_K_2021) and was carried out in accordance with the declaration of Helsinki for medical research involving human subjects. For all autopsies, legal authorization was obtained from the next of kin of the deceased person.

2.2. Study Inclusion and Exclusion Criteria

The only inclusion criterion in our study was the autopsy of confirmed COVID-19 patients, i.e., with at least one positive SARS-CoV-2 PCR test during the disease course. In our study, all subjects were positively tested both before death (RT-PCR for SARS-CoV-2 RNA from nasopharyngeal swab) and after death (RT-PCR for SARS-CoV-2 RNA from cut lung surface swab or FFPE tissue). Accordingly, the exclusion criteria were autopsy cases without positive clinical tests for SARS-CoV-2 RNA or protein.

2.3. Study End-Points

Given the retrospective autopsy study, we had no defined end-points of the study, apart from analyses of viral spread in various tissues and pathological analyses of organ injury.

2.4. Histology Samples and Cohort Description

We used tissue collected from eight autopsies (Table 1). At the time of death, patients were 68 ± 9.55 years old and predominantly male (M:F = 5:3). All patients tested positive for SARS-CoV-2 by RT-PCR during their clinical course. After death, corpses were cooled at 4 °C from 4 h after death until autopsy. The post-mortem interval (i.e., time from death to autopsy) ranged from 20 to 48 h (median, 35.5 h). Autopsies were performed in a dedicated room equipped with a separate ventilation system. All autopsies were performed in two steps, with internal organs removed first and then fixed in 4% buffered formalin and without brain autopsy to avoid aerosol formation. Organs were fixed for one week before further processing. Then, all organs from the thorax and abdomen were examined macroscopically and microscopically (tongue, oropharynx, tonsil, salivary gland, thyroid, proximal and distal trachea, paraaortal/cervical/hilar/abdominal lymph nodes, each lung lobe (one central and one peripheral sample each), heart (anterior, lateral and posterior left ventricular wall, septum, left ventricular papillary muscles, and right ventricle), esophagus, stomach, small intestine, colon, left and right liver lobes, pancreas, spleen, left and right kidney, left and right adrenal gland, uterus (f)/prostate (m), ovary (f)/testis (m), muscle, and skin. Personal protective equipment included N95 masks, waterproof protective suits, goggles, waterproof aprons, and multiple layers of gloves. All garments were changed before and after autopsies were performed. The detailed protocol of the autopsy procedure is available at https://www.pathologie-dgp.de/media/Dgp/aktuelles/Anl._3_Obduktion_COVID-19_15042020__1_.pdf (accessed on 20 June 2021) (in German). We have also used an independent validation cohort of nine cases described in detail in the supplementary methods.

2.5. Histopathological Examination

For microscopic examination, all formalin-fixed specimens were dehydrated and paraffin-embedded (formalin-fixed and paraffin-embedded—FFPE), cut into 4 µm thin slices, and stained on an autostainer according to standard protocols with hematoxylin-eosin (HE) stain. All slides were digitized using the Aperio AT2 brightfield scanner (Leica Biosystems, Nussloch, Germany) with a 40x objective generating Whole Slides Images (WSI).

2.6. Tissue Microarray (TMA) Block Preparation

For FISH analysis, tissue microarrays were created from 25 organs (oropharynx, tonsil, salivary gland, thyroid, distal trachea, perihilar/mesenteric lymph node, lung (left and right, two central and one peripheral), heart (anterior, left ventricle wall), esophagus, stomach, large/small intestine, liver, pancreas, spleen, kidney, adrenal gland, urinary bladder, uterus/prostate, ovary/testis, bone marrow, muscle, and skin; Supplementary Table S1). Punches for tissue microarrays (3 mm diameter) were taken under HE-morphologic control to obtain areas with the least autolytic changes or most representative areas for specific pathologic changes (e.g., hyaline membranes, squamous metaplasia in the lung, neoplastic cells in malignant disease). TMAs were then sectioned with a microtome sequentially for various stains, including hematoxylin-eosin (HE) and in situ hybridization, as mentioned below.

Table 1. Patient characteristics of our COVID-19 study cohort.

Patient	Sex	Age Range (y)	BMI	Smoker	Diabetes (Yes, Type/No)	Hypertension (Yes/No)	Antidiabetic/ Antihypertensive Medication	First Symptoms to Death (d)	Hospital Admission to Death (d)	Death to Autopsy (d)	Duration of Ventilation Therapy (d)
1	M	76–80	Moderately obese	Unknown	yes, 1	yes	Insulin, ACE-I, diuretics	7	2	1	0
2	F	71–75	Overweight	Unknown	yes, 2	yes	Anti-DM, ACE-I, Beta-blocker	12	7	1	7
3	M	81–85	Overweight	Personal history of tobacco abuse	yes, 2	yes	AngiotensinRb, Calcium-channel-blocker, Betablocker, NO-releasing vasodilator, Anti-DM, Insulin	12	11	1	7
4	M	56–60	Normal	Unknown	yes, 2	yes	Anti-DM, Beta-blocker	27	24	1	24
5	M	66–70	Overweight	Unknown	no	yes	Not available	35	29	1	29
6	F	71–75	Overweight	Unknown	no	no	Not applicable	38	33	2	32
7	M	55–60	Normal	Unknown	no	no	Not applicable	52	46	2	44
8	F	61–65	Normal	Unknown	no	yes	AngiotensinRb; Beta-blocker	64	60	2	57

BMI = body mass index; d = day; y = year; ACE-I = ACE-inhibitors; AngiotensinRb = angiotensin-receptor-blocker; Anti-DM = antidiabetics (excluding insulin), NO = nitric oxide.

2.7. SARS-CoV-2 RNA Detection with Fluorescence In Situ Hybridization (FISH)

The fresh-cut, 1 µm-thick TMA sections were deparaffinized in xylene and then dehydrated with 100% ethanol. FISH was performed on the sections with the RNAscope® Multiplex Fluorescent Reagent Kit v2 assay (Advanced Cell Diagnostics, Inc., Hayward, CA, USA), based on the assay principle as described [22]. Briefly, we incubated the tissue sections with H_2O_2 and performed a heat-induced target retrieval step followed by protease incubation with the reagents provided. RNA sequences of SARS-CoV-2 S gene, SARS-CoV-2 antisense of S gene, ACE2, and TMPRSS2 were hybridized using RNAscope® probe -V-nCoV2019-S (#848561-C1), -V-nCoV2019-S-sense (#845701-C1), -Hs-ACE2-C2 (#848151-C2) and -Hs-TMPRSS2-C2 (#470341-C2), respectively. Positive (C1: *POLR2A* gene of *Homo sapiens*; C2: *PPIB* gene of *Homo sapiens*) and negative probes (*dap* gene of *Bacillus subtilis*) were also applied in each experiment. After the amplifier steps, according to the manual, Opal™ 570 and 650 fluorophores (PerkinElmer Life and Analytical Sciences, Boston, MA, USA) were applied to the tissues incubated with C1 and C2 probes, respectively. Finally, nuclei were labelled with DAPI, and the slides were mounted with ProLong™ Gold antifade reagent (Invitrogen, Waltham, MA, USA). Sections were analyzed with Zeiss Axio Imager 2 and image analysis software (ZEN 3.0 blue edition).

2.8. Electron Microscopy (EM)

Samples prepared for transmission electron microscopy were obtained after 7–10 days of formalin fixation and additional fixation in 3% glutaraldehyde for 24 h. Samples were post-fixed in 1% OsO_4 (Roth, Karlsruhe, Germany) and dehydrated in ascending ethanol series (30%, 50%, 70%, 90%, and 100%). Dehydrated samples were incubated in propylene oxide (Serva, Heidelberg, Germany) and embedded in Epon resin (Serva, Heidelberg, Germany). Ultrathin sections were contrast-enhanced by staining with 0.5% uranyl acetate and 1% lead citrate (both EMS, Munich, Germany) and viewed on a transmission electron microscope (Zeiss Leo 906, Oberkochen, Germany).

2.9. Immunohistochemical (IHC) Staining of SARS-CoV-2 Spike Glycoprotein in FFPE Autopsy Lung

We selected autopsy lung samples from a cohort of 3 patient groups, which were diagnosed as ARDS, COVID-19, and influenza a virus subtype H1N1 infection (Table 2). Briefly, 4 µm thin FFPE sections were prepared and deparaffinized in xylene, followed by rehydration with a concentration gradient of ethanol. Tissue sections were then subjected to heat-induced epitope retrieval with Tris-EDTA buffer (pH 9) and quenched with 3% H_2O_2. The slides were then incubated with primary antibody against SARS spike glycoprotein (1:1000; Abcam, Cambridge, UK; Ab272420) in 1% BSA/PBS solution. The remaining IHC steps were performed as previously described [23], and the staining was developed with ImmPACT® VIP Substrate (Vector Labs, Burlingame, CA, USA).

Table 2. List of lung autopsy cohort for testing IHC staining of SARS-CoV-2 spike glycoprotein.

Diagnosis	Sample ID	Autopsy Date	Diffuse Alveolar Damage (DAD) Phase	Spike Protein Stain
ARDS (*n* = 6)	IHC1	June 2010	Exudative/hyaline membranes	Diffuse
	IHC2	April 2011	Fibrotic phase	Diffuse
	IHC3	March 2014	Fibrotic phase	Diffuse
	IHC4	January 2018	Exudative/hyaline membranes	Diffuse
	IHC5	February 2019	Fibrotic phase	Few positive cells
	IHC6	July 2019	Fibrotic phase	Few positive cells
Influenza A (H1N1) (*n* = 4)	IHC7	November 2009	Proliferative/organizing phase	Diffuse

Table 2. *Cont.*

Diagnosis	Sample ID	Autopsy Date	Diffuse Alveolar Damage (DAD) Phase	Spike Protein Stain
	IHC8	March 2010	Proliferative/organizing phase	Diffuse
	IHC9	February 2018	Proliferative/organizing phase	Diffuse
	IHC10	March 2018	Proliferative/organizing phase	Few positive cells
COVID-19 (n = 6)	Patient 1	April 2020	Proliferative/organizing phase	Diffuse
	Patient 4	April 2020	Fibrotic phase	Focal
	Patient 5	April 2020	Proliferative/organizing phase	Diffuse
	Patient 6	May 2020	Proliferative/organizing phase	Diffuse
	Patient 7	May 2020	Proliferative/organizing phase	Focal
	Patient 8	May 2020	No DAD	Diffuse
Normal (n = 6)	IHC17	June 2009	Normal	Negative
	IHC18	June 2009	Normal	Few positive cells
	IHC19	May 2011	Normal/edema	Diffuse
	IHC20	April 2013	Normal	Diffuse
	IHC21	January 2015	Atelectasis	Diffuse
	IHC22	June 2015	Normal	Some positive cells

2.10. RNA Isolation from FFPE Specimens and SARS-CoV-2 RNA Detection

We extracted RNA from FFPE tissue using a Maxwell® 16 LEV RNA FFPE Purification Kit (Promega GmbH, Walldorf, Germany) on the Maxwell® 16 IVD instrument (Promega GmbH) or with the ReliaPrep™ FFPE Total RNA Miniprep System (Promega GmbH) according to the manufacturer's instructions. We stored the RNA samples at −80 °C until further processing.

Previously we compared two different kits for RT-PCR analysis [24]. Here, we used the TaqMan™ Fast 1-Step Master Mix (Thermo Fisher Scientific GmbH, Dreieich, Germany) for the qualitative detection of the E gene (encoding envelope protein) of severe acute respiratory syndrome coronavirus type 2 (SARS-CoV-2) by a primer pair (0.4 µM) and probe (0.2 µM) set labelled with fluorescent reporters and quencher dyes. We used TaqMan® Exogenous Internal Positive Control reagents (Thermo Fisher Scientific GmbH, Dreieich, Germany) as internal PCR controls. RT-PCR was performed as previously described [24,25]. Briefly, we reversely transcribed (50 °C for 10 min) and amplified the RNA extracted from FFPE tissues with the reaction mixture at 95 °C for 20 s and followed by 45 cycles of 95 °C for 3 s and 58 °C for 30 s. We used the Amplirun® SARS-CoV-2 RNA control (Bestbion dx GmbH, Cologne, Germany) provided with 13,000 viral RNA copies μL^{-1} to calculate the viral RNA copies in the tissue samples. In our SARS-CoV-2 positive tissues, the third quartile of the detectable viral copies is 328 viral copies μL^{-1}, which is equivalent to the Ct value of 30.7. In this regard, we defined the cut-off value indicating a high viral load of SARS-CoV-2 in the sample when the Ct value was $\leq$30.7.

3. Results

3.1. Study Cohort

The main characteristics of the study cohort (5 male/3 female; median age 69 (55–83) years) are given in Table 1. The period between the onset of symptoms and death ranged from 12 to 64 days (median 31 days, Figure 1), thereby including early and late/prolonged disease stages. The time between the onset of symptoms and admission ranged from 1 to 7 days (median 5 days, Figure 1) and from admission to death was 2 to 60 days (median 26.5 days, Figure 1). Six patients had at least one clinically confirmed comorbidity, including hyper-

tension (n = 5), diabetes mellitus type 2 (n = 3) or type 1 (n = 1), coronary artery disease (n = 2), malignant disease (n = 1), liver cirrhosis (n = 1) and dementia (n = 1). One patient had a history of chronic kidney disease with kidney transplant and immunosuppression. One patient had a history of tobacco abuse, while no information of current or previous tobacco abuse was available for the remaining 7 patients. None of the patients had tested positive for the respiratory syncytial virus or influenza A and B viruses upon admission. Seven patients were treated with mechanical ventilation, of which three patients were treated with additional extracorporeal membrane oxygenation (ECMO) subsequently. One patient refused mechanical ventilation and intensive care treatment. Duration of ECMO treatment ranged from 342 to 1381 h (median 568 h). During treatment, five patients had an acute kidney injury and required dialysis. None of the patients had a cerebrovascular disease or chronic obstructive pulmonary disease (COPD).

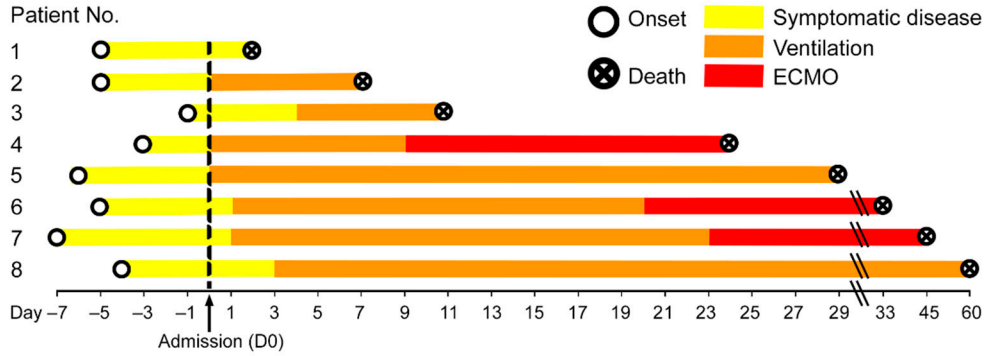

Figure 1. Disease duration of the patient cohort in our study. The disease course of each of the eight COVID-19 patients is shown from disease onset until death. Hospital admission was denoted as day 0, the therapies are color-coded. Patient 1 had the shortest time between the beginning of symptomatic disease and death, i.e., six days, while patient 8 had the longest disease course till death with eight weeks of mechanical ventilation.

3.2. Pathological Findings

From the autopsy analyses, the direct cause of death in all patients was diffuse alveolar damage (DAD) with mixed and overlapping patterns of the exudative, proliferative, and organizing phase or fibrotic phase (Supplementary Table S2). All patients had heavier lungs compared to the normal range (median left: 945 g and right: 1191 g, normal: 500–700 g). Intra-alveolar granulocyte infiltration indicating bacterial superinfection was found in the majority of cases (5/8). Additionally, squamous metaplasia (6/8) and multinucleated intra-alveolar giant cells (5/8) were found. Two patients displayed pulmonary artery thrombosis. Some common findings in other organs were ductular cholestasis in the liver (5/8) and cardiomegaly (6/8; median 482 g). All pathological diagnostic data are summarized in Supplementary Table S2.

Pulmonary findings of DAD included hyaline membranes, intra-alveolar edema, proliferative DAD after a disease duration of <21 days in three patients and organizing or fibrotic DAD with bronchiolization and squamous metaplasia after a disease duration of >21 days in five patients (Supplementary Table S2). There was a diffuse distribution of different DAD phases and non-affected tissue, with highly fibrotic areas neighboring next-to-normal appearing regions. Erosive tracheobronchitis was present in two patients. Pulmonary lymph nodes showed enlargement and reactive changes with sinus histiocytosis. Pulmonary metastases from breast or papillary thyroid cancer was found in two patients (Supplementary Figure S2C,D).

No overt pathological findings attributable to SARS-CoV-2 infection could be recognized outside of the lung. In a detailed analysis, two of five patients with a disease duration of >21 days showed signs of borderline myocarditis with >14 CD3 positive lymphocytes/mm^2 (patient 4, 50 CD3+ cells/mm^2 and patient 5, 16 CD3+ cells/mm^2). In

these patients, cardiac tissue was positive for SARS-CoV-2 RNA (Ct value $\geq$ 30 in patient 4 and Ct value $\leq$ 30 in patient 5, Figure 2). In three additional patients with a disease duration of 12- 64 days, CD3 positive lymphocytes were increased to $\geq$10/mm^2 (patient 3 and 8, 10 CD3+ cells/mm^2 and patient 7, 11 CD3+ cells/mm^2). In two of these three cases, the cardiac tissue was positive for SARS-CoV-2 RNA (Ct value $\leq$ 30 in patient 3 and Ct value $\geq$ 30 in patient 7, Figure 2). In the five cases with increased CD3 lymphocytes, also intravascular lymphocytes were increased, consistent with capillaritis (or endotheliitis). In all cases, we found an increased number of intra- and peri-vascular CD68 positive macrophages. Myocyte injury was not found in any case.

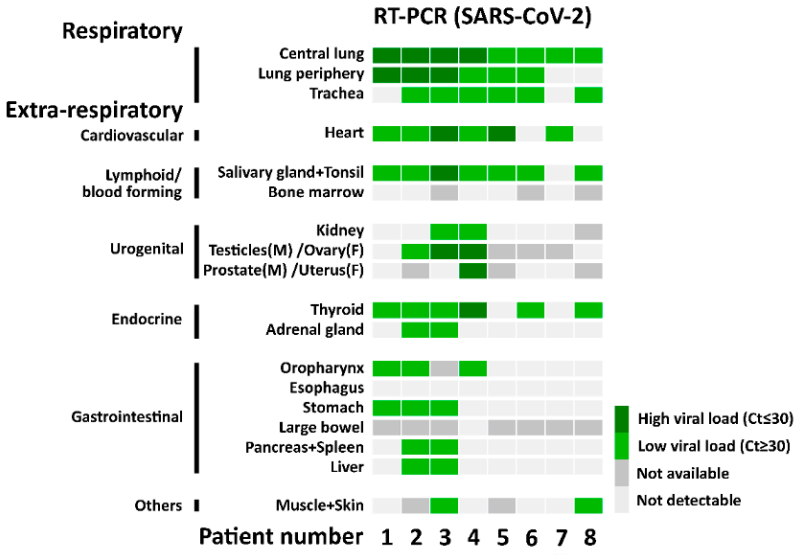

Figure 2. SARS-CoV-2 RNA detection with RT-PCR. The heatmap shows the results of the quantitative PCR detection of SARS-CoV-2 for each patient in all analyzed tissues.

In the haematopoetic system, an increased number of macrophages were visible in the bone marrow of one patient. This patient fulfilled 5 of 8 criteria of the macrophage activation syndrome [26]. The spleen morphologically seemed to be depleted of lymphoid cells in all cases.

In the urogenital system, kidney samples from two patients were positive for RT-PCR of SARS-CoV-2 RNA but displayed no specific pathology (Ct value $\geq$ 30, Patient 3 and 4, Figure 2). In 2/5 males, testicular germ cell aplasia was found. One of these cases was positive for SARS-CoV-2 RNA with high viral load in testicular as well as prostatic tissue (Ct value $\leq$ 30 in Patient 4, Figure 2), while one another case with high viral load in testicular tissue (Patient 3, Figure 2) did not display morphologic alterations of spermatogenesis. In one case of RT-PCR positive ovarian tissue with low viral load (Ct value $\geq$ 30, Patient 2, Figure 2), no pathologic findings were noted.

In the endocrine system, we found moderately to highly increased lymphocytic infiltration in the thyroid of 3/8 patients, two of which were also RT-PCR positive for SARS-CoV-2 RNA (Patient 2 and 6, Figure 2). In 2/8 patients, focal inconspicuous chronic inflammatory cells were found, of which one was associated with high viral load (Ct $\leq$ 30, Patient 4, Figure 2) and one with low viral load (Ct $\geq$ 30, Patient 8, Figure 2). In one patient, we discovered previously unknown advanced papillary thyroid cancer with pulmonary metastasization (Patient 8), as well as a previously unknown papillary thyroid microcarcinoma of 3 mm diameter in a second patient (Patient 5).

In the adrenal gland, 5/8 cases showed inconspicuous chronic inflammation with perivascular distribution (patient 2, 5–8). One case showed moderate chronic inflammation (Patient 3): Two cases were positive for SARS-CoV-2 RNA with RT-PCR (Ct $\geq$ 30, Patient 2 and 3, Figure 2).

In the gastrointestinal system, we detected no specific morphologic alterations, despite positive RT-PCR for SARS-CoV-2 RNA in most samples from the salivary gland, oropharynx, stomach, pancreas, and liver in patients with a disease duration <14 days (Ct $\geq$ 30, Patients 1–3, Figure 2). The liver in Patient 2 showed micronodular cirrhosis. With an increased disease duration of >21 days, three of five patients showed ductular cholestasis of the liver ("cholangitis lenta", Patient 4, 5 and 7, Figure 2), negative for SARS-CoV-2 RNA tested with RT-PCR. Finally, in muscle and skin, we found no specific alterations in two samples positive for SARS-CoV-2 RT-PCR in comparison to those that were negative.

3.3. FISH-Based Detection of SARS-CoV-2, ACE2, and TMPRSS2

RT-PCR allows fast screening of tissues for SARS-CoV-2 positivity, and thereby effective correlation of pathological findings with viral presence. However, it does not allow cell-specific analyses of localization. For this purpose, we validated a FISH method with positive and negative controls by detecting endogenous human genes *POLR2A* and *PPIB)* and a bacterial gene (*dap* gene of *Bacillus subtilis)*, respectively (Supplementary Figure S1A–E). We also validated the probes against the SARS-CoV-2 S gene and human *ACE2* gene on autopsy lung tissue collected from an influenza A (H1N1) infected patient before the COVID-19 pandemic, showing no signal for SARS-CoV-2 S gene and prominent signal for *ACE2* (Supplementary Figure S1F). FISH was performed to analyze tissue microarrays (TMA), followed by HE staining on consecutive slides for the overlay to allow a detailed morphological correlation (Figures 3–7). We used two probe combinations for the FISH detection, either the SARS-CoV-2 S gene sense (determining viral genomic RNA) and ACE2 or the SARS-CoV-2-S gene antisense strand (indicating replicating virus) and TMPRSS2.

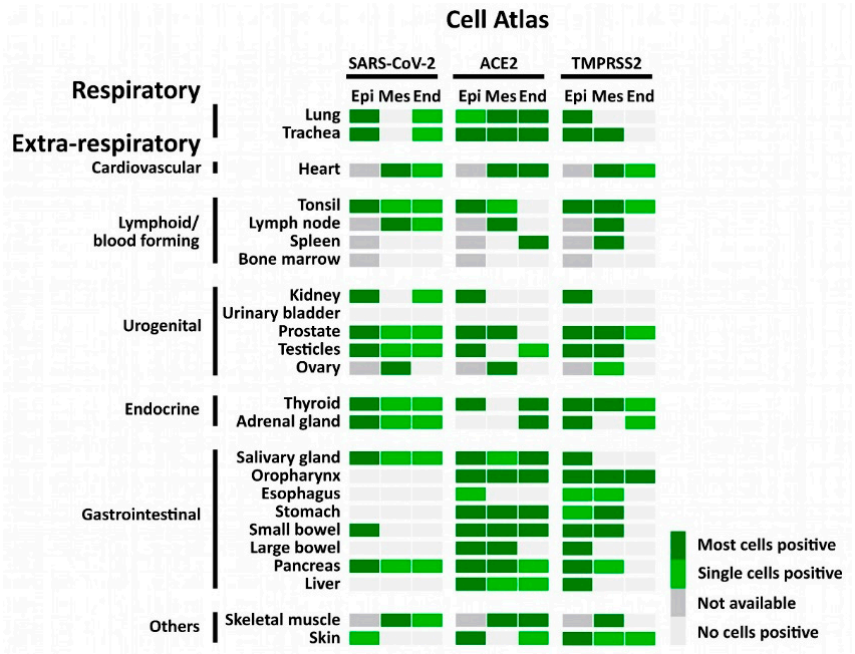

Figure 3. Atlas of cells that were positive for SARS-CoV-2, ACE2, and TMPRSS2 using FISH. The heatmap shows the pattern of SARS-CoV-2, expression of ACE2 and TMPRSS2 in different tissues. Epi = epithelial cells; Mes = mesenchymal stromal cells; End = endothelial cells; not available = tissue does not contain cell type.

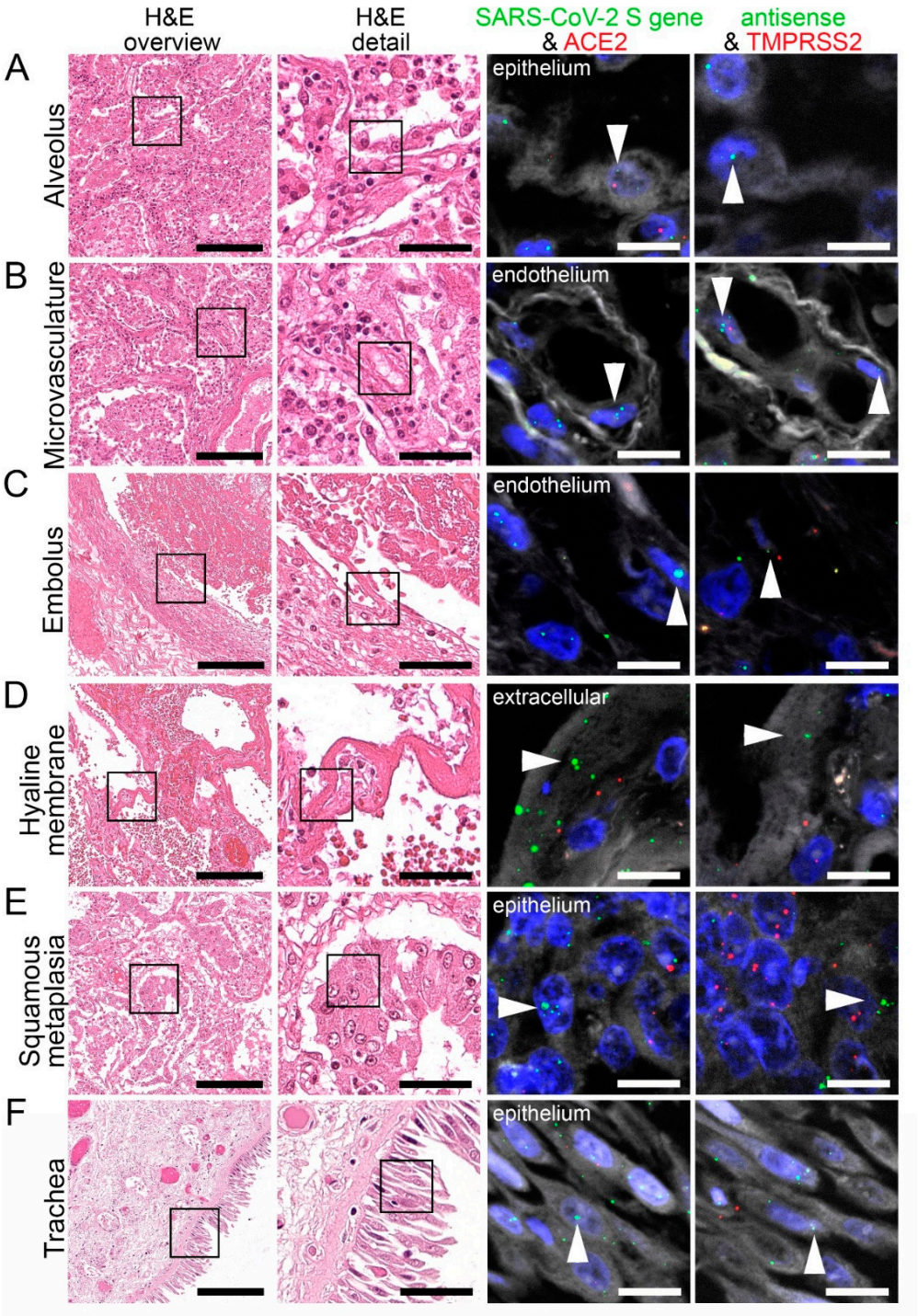

Figure 4. Virus detection in the respiratory system by FISH. HE stained lung tissue and representative image sections showing FISH co-visualization of RNA sequences either of SARS-CoV-2 S gene genomic RNA (green, arrowhead) and ACE2 (red) or SARS-CoV-2 antisense strand RNA as an indicator of replicating virus (green, arrowhead) and TMPRSS2 (red). Morphological details are shown in regions of the alveolus (**A**, alveolar pneumocytes), endothelium in the alveolar wall (**B**), endothelial cells adjacent to an embolus (**C**), hyaline membrane (**D**), squamous metaplasia (**E**, metaplastic epithelium), and trachea (**F**, respiratory epithelium). Scale bars represent 200, 50 and 10 μm, respectively.

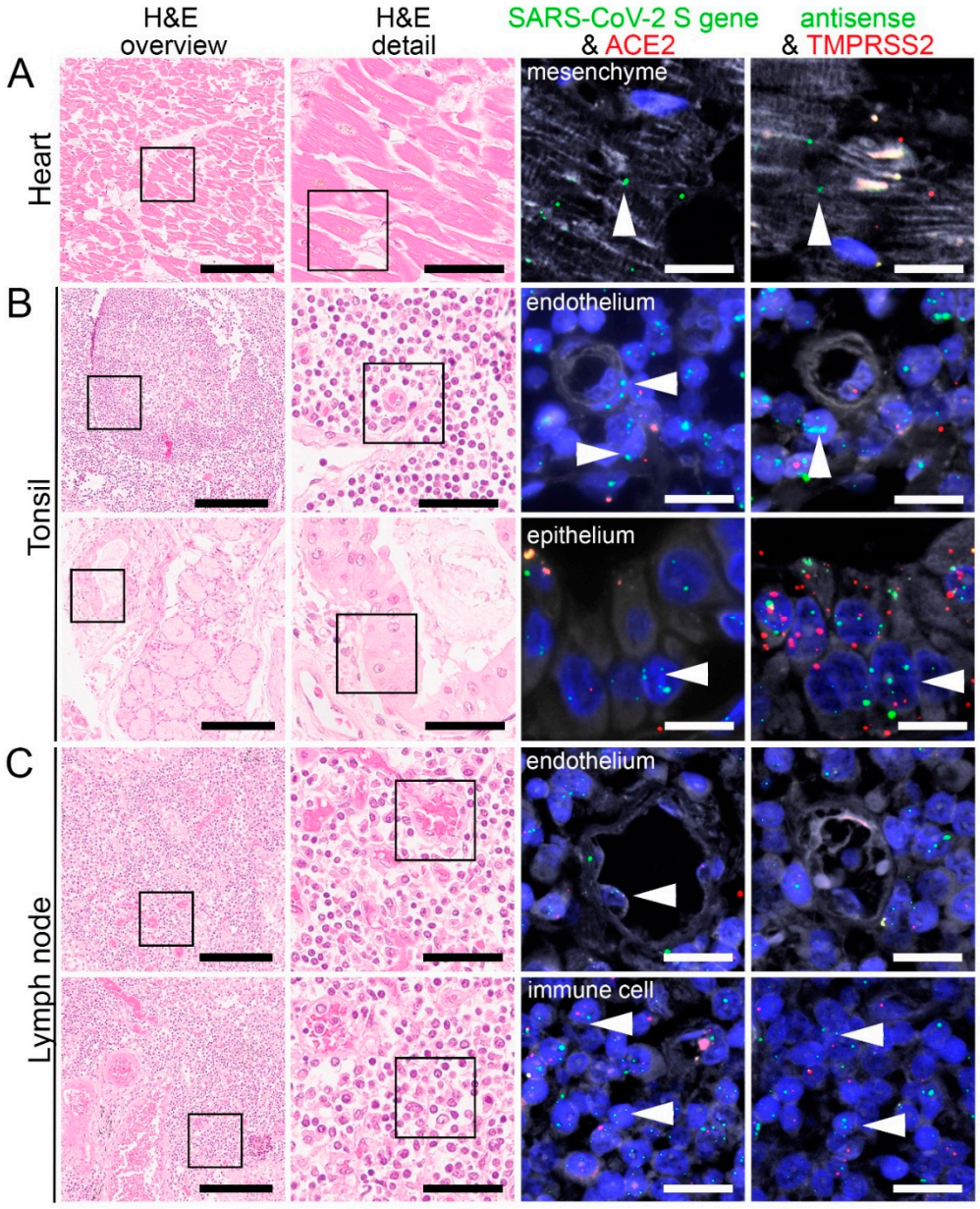

Figure 5. Virus detection in heart and lymphoid organ autopsy tissue by FISH. HE stained tissue and representative image sections showing FISH co-visualization of RNA sequences either of SARS-CoV-2 S gene genomic RNA (green, arrowhead) and ACE2 (red) or SARS-CoV-2 antisense strand RNA indicating replicating virus (green, arrowhead) and TMPRSS2 (red) in the heart (**A**, cardiomyocyte), tonsil (**B**, upper panel: capillary with endothelial lining, surrounded by lymphocytes/immune cells; lower panel: local small salivary gland epithelium) and lymph node (**C**, upper panel: capillary with endothelial lining; lower panel: lymphocytes/immune cells). Scale bars represent 200, 50 and 20 μm, respectively.

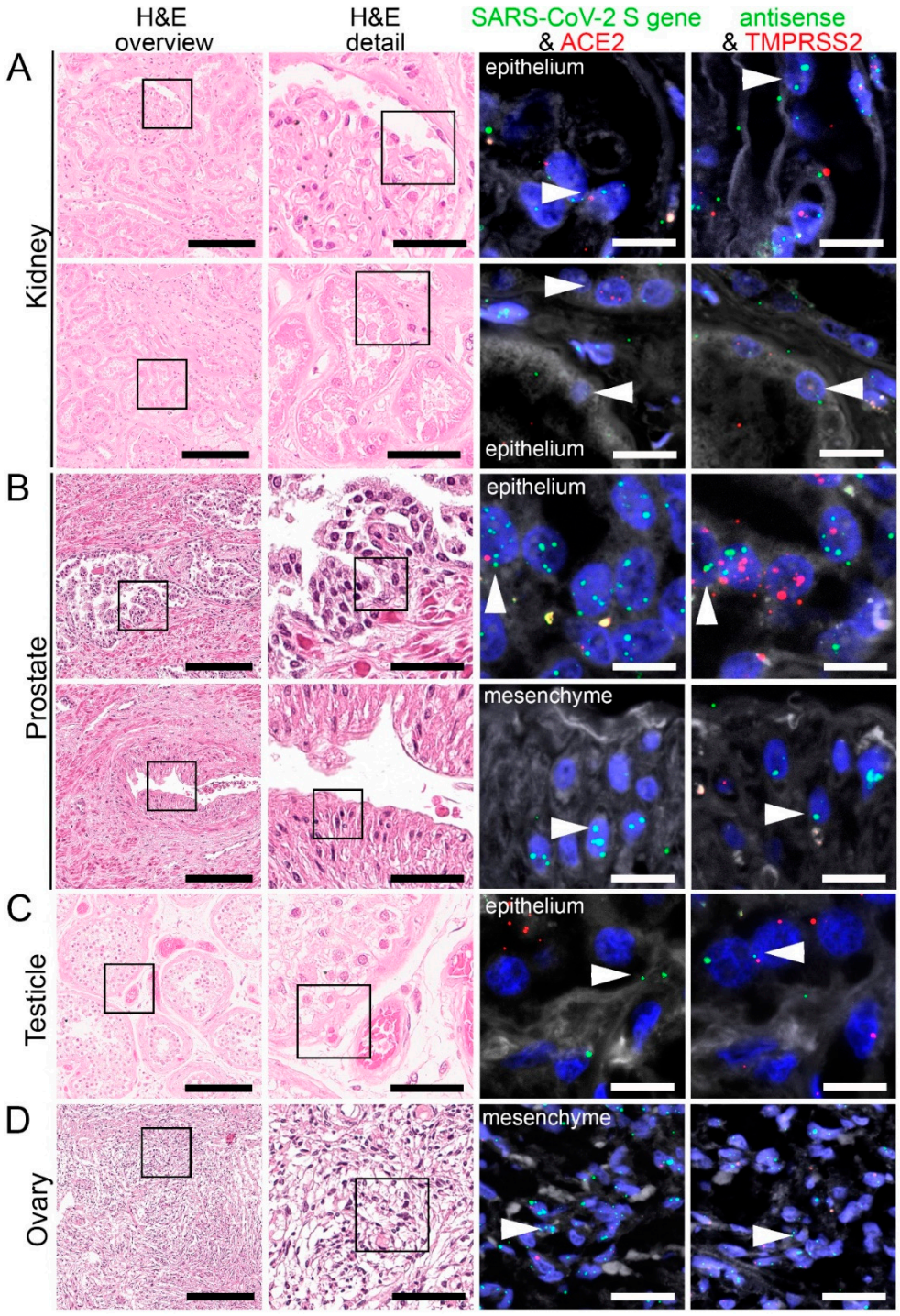

Figure 6. Virus detection in urogenital tract autopsy tissue by FISH. HE stained tissue and representative image sections showing FISH co-visualization of RNA sequences either of SARS-CoV-2 S gene genomic RNA (green, arrowhead) and ACE2 (red) or SARS-CoV-2 antisense strand RNA as an indicator of replicating virus (green, arrowhead) and TMPRSS2 (red) in the kidney (**A**, upper panel: glomerular visceral epithelial cells/podocytes; lower panel: tubular epithelial cells), prostate (**B**, upper panel: glandular epithelial cells; lower panel: vascular smooth muscle cells), testicle (**C**, germinal epithelium) and ovary (**D**, mesenchymal stromal cells). Scale bars represent 200, 50 and 20 µm (**A**,**C**,**D**) or 10 µm (**B**), respectively.

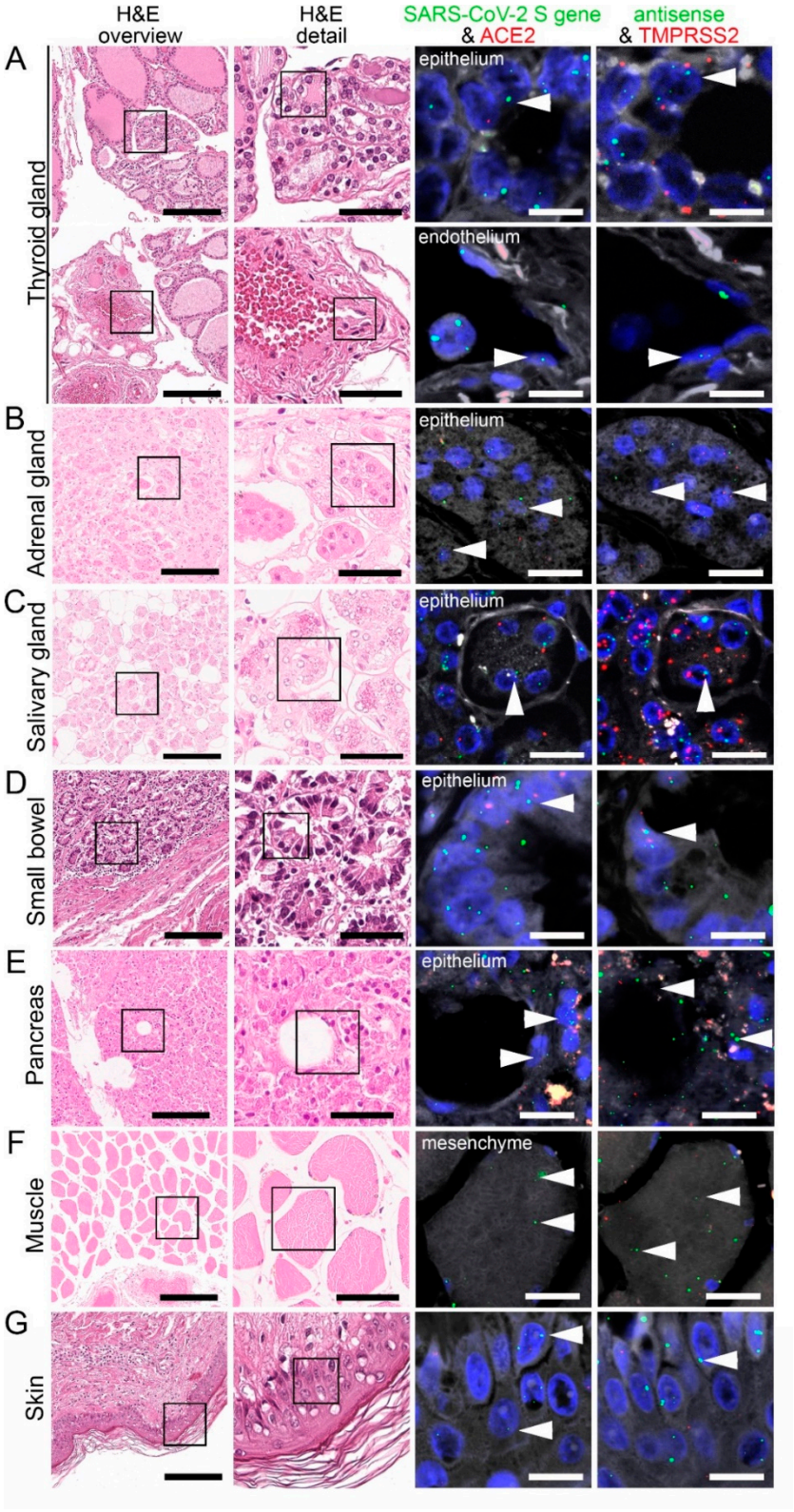

Figure 7. Virus detection in endocrine and gastrointestinal organs and skeletal muscle autopsy tissue by FISH. HE stained tissue and representative image sections showing FISH co-visualization of RNA sequences either of SARS-CoV-2 S gene genomic RNA (green, arrowhead) and ACE2 (red) or SARS-CoV-2 antisense strand RNA indicating replicating virus (green, arrowhead) and TMPRSS2 (red) in the thyroid (**A**, upper panel: follicular epithelium; lower panel: vascular endothelium), adrenal gland (**B**, glandular epithelium), salivary gland (**C**, acini), small bowel (**D**, crypt epithelium), pancreas (**E**, acinar epithelium), skeletal muscle (**F**, skeletal muscle cell) and skin (**G**). Scale bars represent 200, 50 and 10 μm (**A**,**C**,**F**) or 20 μm (**B**,**D**,**E**), respectively.

Consistent with the RT-PCR results, we identified SARS-CoV-2 positive signals in the lung and respiratory tract (Figure 4, Supplementary Figure S2), heart, lymphoid organs (Figure 5), urogenital tract (Figure 6), endocrine and gastrointestinal organs, muscle and skin (Figure 7). We also observed the positive signal for the replicating SARS-CoV-2 (antisense) in all these organs. The SARS-CoV-2 receptor ACE2 and protease TMPRSS2 RNA were found in all organs except bone marrow and urinary bladder (Figure 3).

3.4. SARS-CoV-2, ACE2, and TMPRSS2 in the Respiratory System

We have identified several respiratory cells that were positive for SARS-CoV-2 genomic (S gene; sense) and replicating (S gene: antisense) RNA, ACE2, and TMPRSS2. This included the bronchial and alveolar epithelial cells and cells of the squamous metaplasia in the lung (Figure 4A,E, Supplementary Figure S2A). In the microvasculature, SARS-CoV-2 genomic and replicating RNA could be found in the endothelial cells together with ACE2 and TMPRSS2 (Figure 4B). SARS-CoV-2 genomic and replicating RNA, and TMPRSS2 RNA was also detected in the endothelium adjacent to emboli within vessels (Figure 4C).

In the patients with pulmonary metastases from breast cancer and papillary thyroid cancer, some of the cancer cells were positive for SARS-CoV-2 genomic and replicating RNA, ACE2, and TMPRSS2 RNA (Supplementary Figure S2B,C).

In one lung sample, giant cells were positive for SARS-CoV-2 genomic and replicating RNA, and few were positive for ACE2 RNA (Supplementary Figure S2D). FISH also indicated some neutrophils to be positive for SARS-CoV-2 genomic and replicating RNA, ACE2, and TMPRSS2 RNA (Supplementary Figure S2E). Furthermore, hyaline membranes were positive for SARS-CoV-2 genomic and replicating RNA (Figure 4D), likely originating from detached pneumocytes. Finally, we showed that SARS-CoV-2 genomic and replicating RNA, and TMPRSS2 RNA were found in tracheal epithelial cells (Figure 4F).

3.5. SARS-CoV-2, ACE2, and TMPRSS2 in the Heart, Lymphoid Organs, and Urogenital Tract

Using PCR, we detected SARS-CoV-2 RNA in six out of eight patients in the heart (Figure 2). We found both SARS-CoV-2 genomic and replicating RNA to be present in cardiomyocytes showing that the virus can infect and replicate in cardiomyocytes (Figure 5A). ACE2 was mainly expressed in the stromal cells and capillary endothelial cells, whereas TMPRSS2 expression was mainly found in perivascular cells and some cardiomyocytes (Figure 5A).

In tonsils, we detected SARS-CoV-2 genomic and replicating RNA in the epithelium, which also expressed ACE2 and TMPRSS2 (Figure 5B; lower panel). Some lymphocytes also showed replicating SARS-CoV-2 RNA (Figure 5B; upper panel). We also observed that ACE2 and TMPRSS2 RNA were expressed by some submucosal cells. In some endothelial cells, we detected only TMPRSS2 RNA but not ACE2 RNA (Figure 5B; upper panel).

In both perihilar and mesenteric lymph nodes, we observed most mesenchymal stromal cells and immune cells to be positive for SARS-CoV-2 genomic and replicating RNA (Figure 5C; upper panel). Some endothelial cells were also infected by the virus (Figure 5C; SARS-CoV-2 genomic RNA, upper panel). Additionally, both ACE2 and TMPRSS2 RNA were expressed strongly in the immune cells within the lymph nodes.

In kidneys, we detected SARS-CoV-2 in different epithelial cells, i.e., glomerular podocytes and parietal epithelial cells (Figure 6A; SARS-CoV-2 genomic RNA, upper panel) and tubular epithelial cells (Figure 6A; lower panel). Similar to lungs, renal endothelium was also infected by the virus, both in glomerular and peritubular capillaries (data not shown).

We detected SARS-CoV-2 also in the prostate, localizing in most prostatic glands, particularly in the glandular epithelial cells (Figure 6B; SARS-CoV-2 genomic and replicating RNA, upper panel). Some mesenchymal cells (Figure 6B, SARS-CoV-2 genomic RNA, bottom panel) and endothelial cells were also infected. ACE2 RNA expression was also found in most glandular epithelial cells (Figure 6B; upper panel) and stromal cells. TMPRSS2

RNA was mainly expressed in the glandular epithelium and stromal cells (Figure 5B) and to a much lesser extent in the endothelial cells.

By RT-PCR, we detected a high viral load of SARS-CoV-2 in the testicles. FISH staining indicated that SARS-CoV-2 genomic and replicating RNA were localized mainly in the germinal epithelium (Figure 6C). Some endothelial cells were also infected by the virus. We observed ACE2 RNA was mainly expressed in the Leydig cells and some endothelial cells, whereas TMPRSS2 was mainly found in the stromal cells. SARS-CoV-2 antisense RNA could also be found in stromal cells of the ovary in one COVID-19 patient (Figure 6D), where ACE2 RNA was also mainly expressed, and some stromal cells expressed TMPRSS2 RNA.

3.6. SARS-CoV-2, ACE2, and TMPRSS2 in the Endocrine and Gastrointestinal Organs, Skeletal Muscle, and Skin

Within the endocrine system, there were six infected thyroids within our autopsy cohort. We detected SARS-CoV-2 genomic and replicating RNA in most follicular epithelial cells (Figure 7A; upper panel), some stromal and endothelial cells (Figure 7A; bottom panel). ACE2 RNA was mainly found in the follicular epithelium (Figure 7A; upper panel) and endothelial cells, whereas TMPRSS2 RNA was expressed in most follicular epithelial cells (Figure 7A; upper panel), some stromal and endothelial cells.

In the two adrenal glands, we observed SARS-CoV-2 genomic and replicating SARS-CoV-2 RNA in most glandular epithelial cells (Figure 7B) and to a lesser extent in stromal and endothelial cells. ACE2 RNA expression was mainly found in most endothelial cells. TMPRSS2 RNA was mainly expressed in glandular epithelial cells (Figure 7B) and some endothelial cells.

In the salivary gland, SARS-CoV-2 genomic and replicating RNA were detected in most acini and salivary ducts together with strong detection of ACE2 and TMPRSS2 RNA (Figure 7C). SARS-CoV-2 genomic RNA was also found in some stromal cells and endothelial cells. ACE2 RNA expression was found in some stromal cells and most endothelial cells, but TMPRSS2 RNA was not found in these two cell types.

Within the small bowel, SARS-CoV-2 genomic and replicating SARS-CoV-2 RNA were mainly detected in the enterocytes, accompanied by strong expression of ACE2 and TMPRSS2 RNA (Figure 7C). Additionally, ACE2 RNA expression was found in mesenchymal stromal cells, muscle cells expressed both ACE2 and TMPRSS2 RNA. In the endothelial cells, we detected ACE2 but not TMPRSS2 RNA.

In the pancreas, we detected genomic and replicating SARS-CoV-2 RNA in most acinar cells, which co-localized with strong expression of ACE2 and TMPRSS2 RNA (Figure 7D). SARS-CoV-2 genomic RNA was also detectable in some stromal and endothelial cells. ACE2 RNA was present in most stromal cells and some endothelial cells, while TMPRSS2 RNA was only present in some stromal cells.

We detected genomic and replicating SARS-CoV-2 RNA in the skeletal muscle, mainly localized in the myocytes (Figure 7E) and some endothelial cells. Moreover, the muscle cells also expressed ACE2 RNA and TMPRSS2 RNA. In the endothelial cells, we observed ACE2 RNA expression but not TMPRSS2 RNA.

Finally, we detected both SARS-CoV-2 genomic and replicating RNA in the dermal epithelial cells (Figure 7F). The epithelial cells also expressed ACE2 and TMPRSS2, while mRNA for both proteins was only sparsely detected in endothelial cells.

3.7. IHC of SARS-CoV-2 Spike Glycoprotein on FFPE Autopsy Lung Samples

Protein detection of SARS-CoV-2 spike glycoprotein is widely used in studies in FFPE tissues. We stained for the SARS-CoV-2 spike glycoprotein in the COVID-19 autopsy lung and selected the most commonly used antibodies based on previous studies [24,27], targeting the SARS spike glycoprotein (Abcam, ab272420) and SARS-CoV SΔ10 within S2 domain protein (Genetex, GTX632604). We have tested these two antibodies on FFPE autopsy lung tissues with four different antigen retrieval methods, as outlined in the methods section. All approaches were unsuccessful, i.e., no positive signals could be observed, except the

ab272420 using Tris-EDTA buffer (pH 9) antigen retrieval. We validated this protocol on autopsy lung tissues from our COVID-19 cohort and non-COVID-19 cases as negative controls, including (1) four patients infected with influenza, (2) six patients who developed ARDS (selected non-superinfected areas), and (3) six patients who had no pulmonary pathology (Table 2). These autopsy tissues were collected before the COVID-19 outbreak (from 2009 to July 2019). All lung tissues showed variable but very distinct false-positive unspecific stain, except for a single lung from the non-infected group (Table 2, Figure 8, Supplementary Figure S3). Taken together, IHC based detection of SARS-CoV-2 using the two mentioned antibodies and protocols were not possible to establish or not specific to detect the virus in FFPE tissues.

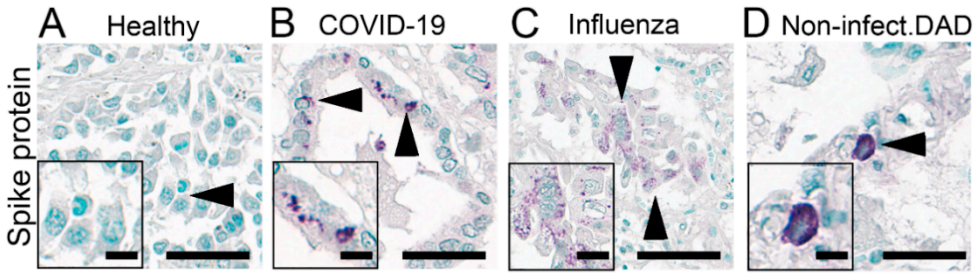

Figure 8. Immunohistochemical staining of SARS spike glycoprotein. IHC staining of SARS spike glycoprotein (#Ab272420) in the lung autopsies collected from patients without any respiratory disease (**A**, Healthy; insert: respiratory epithelial cells) and patients infected with COVID-19 (**B**, COVID-19; insert: respiratory epithelial cells), influenza (**C**, Influenza; insert: respiratory epithelial cells) and non-infectious diffuse alveolar damage (**D**, Non-infect.DAD; insert: cell with features of an alveolar macrophage) with apparently (false-) positive staining (arrowhead). Scale bars represent 40 and 10 µm (insert).

3.8. Visualization of SARS-CoV-2 by Electron Microscopy

Ultrastructural tissue preservation in autopsy material was rather poor and hampered virus particle detection by electron microscopy. Autolytic processes before fixation led to cell degradation and strong autolytic vesicle formation, resulting in many virus-like particles, but not a single reliable SARS-CoV-2 detection, despite a thorough analysis of all cases (data not shown).

3.9. Application of Chromogenic In Situ Hybridization on External FFPE COVID-19 Tissue Samples

FISH requires fluorescence microscopes, which might not be available in all pathologies performing autopsies, and the signal also faints with time. Therefore, we also established the chromogenic in situ hybridization (CISH) for SARS-CoV-2 detection (Supplementary method, Supplementary Table S3). We first validated the CISH detection with the same positive and negative control probes used in FISH (Supplementary Figure S4A–D). To validate the compatibility of our ISH detection of SARS-CoV-2 in FFPE autopsies processed externally, we performed CISH staining on an independent autopsy cohort consisting of nine COVID-19 patients received from the Institute of Pathology, Hannover Medical School, Germany (Supplementary Figure S5). We could detect SARS-CoV-2 genomic and replicating RNA in the cardiomyocytes, intra-glomerular and alveolar cells, hepatocytes, pancreatic and enteric epithelial cells, capillary endothelial cells in lymph nodes, and spleen (Supplementary Figure S5A–I). In the vicinity of the SARS-CoV-2 positive signals, we also detected ACE2 and TMPRSS2 RNA in intra-glomerular cells, hepatocytes, alveolar cells, pancreatic and enteric epithelial cells.

4. Discussion

We here comprehensively analyzed SARS-CoV-2 in tissues from clinical autopsies of COVID-19 cases. We compared various methods, suggesting the most effective and useful approaches for SARS-CoV-2 detection in autopsy tissues, focusing on routine processing

in pathology and thereby possibly the most widespread adoption of the methods. Using these methods, we have comprehensively analyzed a multitude of tissues and cells for SARS-CoV-2 presence to perform a detailed correlation of virus presence and potential pathology findings. We described the viral spread in several tissues (i.e., thyroid, adrenal gland, prostate, large bowel and ovary) that were previously not described and pinpoint the localization to specific cells within each tissue.

Comparing various approaches routinely used in pathology institutes, the RNA detection methods (either by RT-PCR, FISH or CISH) were proved to be the most effective, specific, and suitable to use. In contrast, both immunohistochemistry and electron microscopy turned out not to be suitable, confirming previous reports [16,28,29]. False-negative test results cannot be excluded, neither in the RT-PCR nor the FISH analyses. This seems not to be strongly dependent on RNA quality or quantity [24]. Importantly, we performed all analyses on material that was previously selected as suitable by pathologists (documented by the figures showing the results of the FISH analyses). Additionally, we tested two different target genes in the RT-PCR analyses.

When using RNA-based methods, a 2-step approach could be applied. First, screening the cases and tissues using the RT-PCR, followed by a more complex and time-consuming FISH approach only in positive tissues. We focused our approach on FFPE tissue since this is the most widely adopted tissue processing in most international institutes of pathology and autopsy centers. Although formalin fixation and paraffin embedding might lead to additional RNA degradation, FFPE material has the important advantage of not being infectious and conservable, making further processing much easier and more broadly applicable compared to, e.g., fresh infectious tissue. Furthermore, reliable detection in FFPE materials allows for fast retrospective analysis, as FFPE blocks are regularly archived and widely available in all institutes of pathology.

Compared to RT-PCR, the ISH detection method in FFPE autopsies could avoid the interference of SARS-CoV-2 RNA in the blood that remained within the tissues [14]. To precisely localize the signal, consecutive sections can be used, allowing a very detailed association of morphology with positive signals, which is impossible in FISH or CISH sections alone. Apart from the precise localization, the FISH approach also allows co-localizing analysis of the viral RNA and its targets ACE2 and TMPRSS2 on the cellular level. Compared to FISH, the CISH method has some advantages, particularly not requiring fluorescence microscopy equipment which might not be readily available in all institutes, longer stability of the signals, and the possibility of a faster digitalization of the slides using whole-slide scanners. On the other hand, the FISH signals are easier to detect and provide a much better signal-to-noise ratio by adjusting the fluorescence excitation. Validation of the ISH on an independent external cohort in our study confirmed its broad applicability.

The macroscopic and microscopic findings of the autopsy lungs are entirely in line with previous reports on pulmonary and upper airway findings in COVID-19 [16,25,30,31] and SARS-CoV-1 autopsies [32,33]. The strong positivity for viral RNA, including the antisense, as well as the co-localization with ACE2 and TMPRSS2, associated the pathological findings with the viral presence and are also in line with previous reports. We here provided comprehensive morpho-molecular analyses and examples of the localization of the virus in various cells and compartments of the lung (i.e., squamous metaplasia and giant cell), which were previously not reported.

Currently, COVID-19 is considered a multisystemic disease. Our data, showing the viral presence, including replicating virus in the majority of analyzed tissues, might confirm this hypothesis. However, in our macroscopic and microscopic evaluation of all extra-respiratory organs, we were not able to identify specific pathological alterations that would be attributable to viral infection. We cannot exclude subtle or molecular changes that were not translating to the morphological changes presented in the infected non-respiratory tissues. However, our detailed analyses might suggest that the SARS-CoV-2 spreading beyond the respiratory tract does not induce any major pathology and might be rather negligible in comparison to the pulmonary involvement, at least in fatal cases.

An alternative explanation for the diverse pathological alterations could also be due to individual pathophysiological characteristics and differences between the study subjects, which were not reflected by the available clinical data. Given the small size of our cohort, the different disease stages of the study subjects could also explain the variability. Similar conclusions were also suggested in some previous reports [15,25,34].

One hypothesis for the multisystemic nature of COVID-19 is the systemic spread and effects on the (micro)vasculature [35]. We showed that the SARS-CoV-2 genomic and replicating RNA and particularly TMPRSS2 RNA in the endothelial cells of vessels across all organs, supporting this hypothesis. This is supported by the data showing SARS-CoV-2 RNA in the blood [36]. Besides, we also found the viral RNA in vessels across all organ systems and pulmonary endothelial cells adjacent to thrombi, which might be a hint to the microvascular damage induced by direct endothelial infection [15]. However, we have only found vasculature with thrombi in the lungs, but not in any other of the analyzed organs or tissues. This might be influenced by our relatively small cohort, mainly consisting of intensive care unit patients who had been receiving anticoagulative treatment. We have also been very cautious regarding the interpretation of vascular occlusion as intravital thrombotic events in order not to false-positively interpret post-mortem clots as intravital thrombi.

We showed the predominance of viral RNA in ACE2 and/or TMPRSS2- expressing epithelial cells compared to mesenchymal stromal cells and endothelial cells in various organs. This included, e.g., trachea, lung, tonsil, salivary glands, kidney, and small bowel. The presence of SARS-CoV-2 RNA in salivary glands supports the effectiveness of saliva-based SARS-CoV-2 testing that has been emerged worldwide [37]. We also showed the presence of viral RNA in non-epithelial tissues, such as lymph nodes, heart, and skeletal muscle [25,38–40]. We visualized for the first time SARS-CoV-2 viral RNA in exo-/endocrine organs, i.e., in the thyroid, adrenal gland, prostate, testicle, and ovary. Our findings in the testicle are in line with previous reports of SARS-CoV-2 RNA detections in seminal fluid and testicular tissue with RT-PCR [41,42]. Regarding adrenal glands and prostate in COVID-19, microinfarctions, hemorrhage, or thrombosis have been described in COVID-19 autopsies [43,44]. Concerning the thyroid, previous descriptions of follicular epithelial morphologic alterations exist for SARS infection [45], but not COVID-19. We also detected SARS-CoV-2 RNA in cancer cells in two cases of pulmonary metastasis. This finding is in line with a previous report of a positive RT-PCR result in oral cancer tissue of a COVID-19 patient [46]. Current knowledge on the potential impact of SARS-CoV-2 infection in cancer cells remains incomplete, beyond the observation of their higher morbidity and mortality of cancer patients after being infected with the SARS-CoV-2 virus [47].

We could also confirm the presence of ACE2 receptor in alveolar epithelial cells [48] and pancreatic ductal cells [49] as well as TMPRSS2 in salivary acinar cells [50] and prostate epithelial cells [51] as previously suggested by single-cell RNA sequencing studies.

In conclusion, our present study suggests that RT-PCR and FISH performed on FFPE tissues are reliable methods allowing tissue and cellular localization in autopsies. We provide a "cellular and whole-body tissue atlas" of organ tropism profile of SARS-CoV-2 in severe COVID-19 patients, suggesting a multisystemic spread in virtually all cell types of infected organs.

5. Study Limitations

Our study has several limitations. We have not found viral presence in a few analyzed tissues, including bone marrow, esophagus, large bowel, and spleen. This might be due to the low number of analyzed patients. We aimed to perform a detailed analysis and cellular localization, which in the absence of reliable protein or ultrastructural detection and required to perform FISH analysis. This method is time-consuming, particularly when using co-localization with consecutive sections, making it hard to apply in a large number of cases. Therefore, for more high-throughput approaches, we suggest pre-screening of the cases and tissues using RT-PCR.

Our study is descriptive and provides a single time-point analysis of only fatal cases. However, these are intrinsic limitations of autopsy studies. On the other hand, there are no other approaches that would allow analyzing comprehensively all human tissues in a comparable way. The variable degrees of autolysis in some tissue samples might limit the efficacy of viral detection. This was particularly true for electron microscopy, which was not applicable in our hands.

Our study and sample acquisition focused on the standard and main tissue processing in pathology and autopsies, i.e., FFPE tissues. This has a big advantage of not being infectious; therefore, it can be processed in virtually all pathology laboratories. In addition, the FISH method allows a cell-specific analysis. The downside is that we cannot perform other methods confirming our findings, e.g., Western blot. Another limitation of our study is that we cannot make sufficiently robust analyses and interpretations regarding the potential role of medication or other modifying factors, e.g., ACE/ACE2 ratio. This is due to our relatively small size cohort, the design of this autopsy study and the different stages of COVID-19 patients being involved.

Methodologically, in some cell types with scarce cytoplasm and overlap with neighboring cells, it was impossible to allocate the ISH signal localization to a particular cell. We found a small population of SARS-CoV-2 positive cells that were negative for ACE2 or TMPRSS2 RNA. This is most likely due to a sampling bias, given that the FISH or CISH slides are extremely thin and only reflect part of the volume of the cells. An alternative explanation might be that SARS-CoV-2 was suggested to enter the host cells independent of ACE2 and TMPRSS2 [52]. Virus positive cells which are negative for ACE2 or TMPRSS2 may acquire viral RNA through phagocytosis of infected cell debris, which could apply for both professional and non-professional antigen-presenting cells, i.e., macrophages, monocytes, neutrophils, dendritic cells, and B cells as well as fibroblasts, and some epithelial and endothelial cells, respectively [53]. Low or no expression of ACE2/TMPRSS2 has been shown in macrophage, lymphocyte and dendritic cell from previous studies [48,54,55]. However, we have observed the positive FISH signals for ACE2 and TMPRSS2 RNA in the immune cells within the lymph nodes. The FISH method is not quantitative, and we have not analyzed the protein expression of ACE2 and TMPRSS2. Therefore, we cannot conclude the exact expression level of ACE2/TMPRSS2 in the immune cells.

Finally, regarding the widespread appearance of SARS-CoV-2 variants lately, it is unclear whether our RNA-targeted approaches would detect them or be interfered by the mutations, despite the fact that a pool of probes for detecting different genomic sites of the SARS-CoV-2 is used in our FISH method.

Supplementary Materials: The following are available online at https://www.mdpi.com/article/10.3390/cells10081900/s1, Supplementary method, External study cohort, Table S1: List of autopsies from different decedents organized in the TMA, Table S2: Major pathological findings in the autopsy cohort, Table S3: Patient characteristics of the external COVID-19 study cohort, Figure S1: Validation of FISH detection on human autopsies, Figure S2: Virus detection in respiratory system by FISH, Figure S3: Virus detection in respiratory system by IHC staining, Figure S4: Validation of CISH detection on external human autopsies, Figure S5: Detection of SARS-CoV-2 sense, antisense, ACE2 and TMPRSS2 on an external sample by CISH.

Author Contributions: D.W.L.W. and M.C.T. performed the FISH and CISH stains; D.W.L.W., B.M.K. and S.D. performed FISH analysis; D.W.L.W. and S.D. performed immunohistochemistry analysis; D.W.L.W., S.D. and B.M.K. created the figures; D.W.L.W., S.D., B.M.K. and S.v.S. wrote the manuscript; E.M.B. performed electron microscopy; R.D.B., C.W., D.J., S.v.S. and S.W. performed autopsies and histological analyses; R.K.-C., C.C., T.B., D.J. and P.B. supervised the autopsy assessment; S.V. and E.D. performed PCR analyses; P.B. had the conceptual idea. All authors have read and agreed to the published version of the manuscript.

Funding: This work was supported by the German Registry of COVID-19 Autopsies (www.DeRegCOVID.ukaachen.de (accessed on 20 June 2021)), funded by the Federal Ministry of Health (ZMVI1-2520COR201), by the Federal Ministry of Education and Research within the framework of the network of university medicine (DEFEAT PANDEMICs, 01KX2021 and STOP-FSGS-01GM1901A), the German Research Foun-

dation (DFG; SFB/TRR219 Project-ID 322900939, BO3755/13-1 Project-ID 454024652, and DJ100/1-1 432698239), the European Research Council (ERC) under the European Union's Horizon 2020 research and innovation program (grant agreement No 101001791), RWTH START-program (125/17 and 109/20) and the grant of the European Research Council (ERC); European Consolidator Grant, XHale to Danny Jonigk (ref. no. 771883).

Institutional Review Board Statement: The study was conducted according to the guidelines of the Declaration of Helsinki, and approved by the Institutional Review Board (or Ethics Committee) of RWTH Aachen University Hospital (EK 304/20: approved on 14-08-2020, EK 119/20: approved on 24-06-2020, EK 092/20: approved on 02-04-2020) and Hannover Medical School (9621_BO_K_2021: approved on 02-02-2021). For all autopsies, legal authorization was obtained from the next of kin of the deceased person.

Informed Consent Statement: Not applicable.

Data Availability Statement: The authors confirm that the data supporting the findings of this study are available within the article and its Supplementary Materials. Additional raw data supporting the findings of this study are available from the corresponding author (P.B.) on request.

Acknowledgments: The excellent technical help of Inge Losen and Simon Otten is gratefully acknowledged. We wish to thank all relatives and legal representatives for giving their consent for the autopsy procedure.

Conflicts of Interest: The authors declare no conflict of interest.

References

1. Cabrera Martimbianco, A.L.; Pacheco, R.L.; Bagattini, A.M.; Riera, R. Frequency, signs and symptoms, and criteria adopted for long COVID: A systematic review. *Int. J. Clin. Pract.* **2021**, e14357. [CrossRef]
2. Wei, J.F.; Huang, F.Y.; Xiong, T.Y.; Liu, Q.; Chen, H.; Wang, H.; Huang, H.; Luo, Y.C.; Zhou, X.; Liu, Z.Y.; et al. Acute myocardial injury is common in patients with COVID-19 and impairs their prognosis. *Heart* **2020**, *106*, 1154–1159. [CrossRef] [PubMed]
3. Sardu, C.; Gambardella, J.; Morelli, M.B.; Wang, X.; Marfella, R.; Santulli, G. Hypertension, Thrombosis, Kidney Failure, and Diabetes: Is COVID-19 an Endothelial Disease? A Comprehensive Evaluation of Clinical and Basic Evidence. *J. Clin. Med.* **2020**, *9*, 1417. [CrossRef] [PubMed]
4. Matarese, A.; Gambardella, J.; Sardu, C.; Santulli, G. miR-98 Regulates TMPRSS2 Expression in Human Endothelial Cells: Key Implications for COVID-19. *Biomedicines* **2020**, *8*, 462. [CrossRef]
5. V'Kovski, P.; Kratzel, A.; Steiner, S.; Stalder, H.; Thiel, V. Coronavirus biology and replication: Implications for SARS-CoV-2. *Nat. Rev. Microbiol.* **2021**, *19*, 155–170. [CrossRef]
6. Sardu, C.; Gargiulo, G.; Esposito, G.; Paolisso, G.; Marfella, R. Impact of diabetes mellitus on clinical outcomes in patients affected by Covid-19. *Cardiovasc. Diabetol.* **2020**, *19*, 76. [CrossRef] [PubMed]
7. Sardu, C.; Maggi, P.; Messina, V.; Iuliano, P.; Sardu, A.; Iovinella, V.; Paolisso, G.; Marfella, R. Could Anti-Hypertensive Drug Therapy Affect the Clinical Prognosis of Hypertensive Patients With COVID-19 Infection? Data From Centers of Southern Italy. *J. Am. Heart Assoc.* **2020**, *9*, e016948. [CrossRef]
8. Maiese, A.; Manetti, A.C.; La Russa, R.; Di Paolo, M.; Turillazzi, E.; Frati, P.; Fineschi, V. Autopsy findings in COVID-19-related deaths: A literature review. *Forensic. Sci. Med. Pathol.* **2020**. [CrossRef]
9. Rensen, E.; Pietropaoli, S.; Weber, C.; Souquere, S.; Isnard, P.; Rabant, M.; Gibier, J.-B.; Simon-Loriere, E.; Rameix-Welti, M.-A.; Pierron, G.; et al. Sensitive visualization of SARS-CoV-2 RNA with CoronaFISH. *bioRxiv* **2021**, 429604. [CrossRef]
10. Gagiannis, D.; Umathum, V.; Bloch, W.; Rother, C.; Stahl, M.; Witte, H.; Djudjaj, S.; Boor, P.; Steinestel, K. Antemortem vs. postmortem histopathological and ultrastructural findings in paired transbronchial biopsies and lung autopsy samples from three patients with confirmed SARS-CoV-2 infection. *medRxiv* **2021**, 20248929. [CrossRef]
11. Shieh, W.J.; Hsiao, C.H.; Paddock, C.D.; Guarner, J.; Goldsmith, C.S.; Tatti, K.; Packard, M.; Mueller, L.; Wu, M.Z.; Rollin, P.; et al. Immunohistochemical, in situ hybridization, and ultrastructural localization of SARS-associated coronavirus in lung of a fatal case of severe acute respiratory syndrome in Taiwan. *Hum. Pathol.* **2005**, *36*, 303–309. [CrossRef] [PubMed]
12. Ackermann, M.; Mentzer, S.J.; Jonigk, D. Visualization of SARS-CoV-2 in the Lung. Reply. *N. Engl. J. Med.* **2020**, *383*, 2689–2690. [CrossRef] [PubMed]
13. Bharat, A.; Querrey, M.; Markov, N.S.; Kim, S.; Kurihara, C.; Garza-Castillon, R.; Manerikar, A.; Shilatifard, A.; Tomic, R.; Politanska, Y.; et al. Lung transplantation for patients with severe COVID-19. *Sci. Transl. Med.* **2020**, *12*, 574. [CrossRef] [PubMed]
14. Bhatnagar, J.; Gary, J.; Reagan-Steiner, S.; Estetter, L.B.; Tong, S.; Tao, Y.; Denison, A.M.; Lee, E.; DeLeon-Carnes, M.; Li, Y.; et al. Evidence of Severe Acute Respiratory Syndrome Coronavirus 2 Replication and Tropism in the Lungs, Airways, and Vascular Endothelium of Patients With Fatal Coronavirus Disease 2019: An Autopsy Case Series. *J. Infect. Dis.* **2021**, *223*, 752–764. [CrossRef] [PubMed]

15. Bussani, R.; Schneider, E.; Zentilin, L.; Collesi, C.; Ali, H.; Braga, L.; Volpe, M.C.; Colliva, A.; Zanconati, F.; Berlot, G.; et al. Persistence of viral RNA, pneumocyte syncytia and thrombosis are hallmarks of advanced COVID-19 pathology. *EBioMedicine* **2020**, *61*, 103104. [CrossRef]
16. Massoth, L.R.; Desai, N.; Szabolcs, A.; Harris, C.K.; Neyaz, A.; Crotty, R.; Chebib, I.; Rivera, M.N.; Sholl, L.M.; Stone, J.R.; et al. Comparison of RNA In Situ Hybridization and Immunohistochemistry Techniques for the Detection and Localization of SARS-CoV-2 in Human Tissues. *Am. J. Surg. Pathol.* **2021**, *45*, 14–24. [CrossRef]
17. Schurink, B.; Roos, E.; Radonic, T.; Barbe, E.; Bouman, C.S.C.; de Boer, H.H.; de Bree, G.J.; Bulle, E.B.; Aronica, E.M.; Florquin, S.; et al. Viral presence and immunopathology in patients with lethal COVID-19: A prospective autopsy cohort study. *Lancet Microbe* **2020**, *1*, e290–e299. [CrossRef]
18. Bouquegneau, A.; Erpicum, P.; Grosch, S.; Habran, L.; Hougrand, O.; Huart, J.; Krzesinski, J.-M.; Misset, B.; Hayette, M.-P.; Delvenne, P.; et al. COVID-19-associated nephropathy includes tubular necrosis and capillary congestion, with evidence of SARS-CoV-2 in the nephron. *Kidney360* **2021**. [CrossRef]
19. Pfister, F.; Vonbrunn, E.; Ries, T.; Jack, H.M.; Uberla, K.; Lochnit, G.; Sheriff, A.; Herrmann, M.; Buttner-Herold, M.; Amann, K.; et al. Complement Activation in Kidneys of Patients With COVID-19. *Front. Immunol.* **2020**, *11*, 594849. [CrossRef]
20. Best Rocha, A.; Stroberg, E.; Barton, L.M.; Duval, E.J.; Mukhopadhyay, S.; Yarid, N.; Caza, T.; Wilson, J.D.; Kenan, D.J.; Kuperman, M.; et al. Detection of SARS-CoV-2 in formalin-fixed paraffin-embedded tissue sections using commercially available reagents. *Lab. Investig. J. Tech. Methods Pathol.* **2020**, *100*, 1485–1489. [CrossRef] [PubMed]
21. Hoffmann, M.; Kleine-Weber, H.; Schroeder, S.; Kruger, N.; Herrler, T.; Erichsen, S.; Schiergens, T.S.; Herrler, G.; Wu, N.H.; Nitsche, A.; et al. SARS-CoV-2 Cell Entry Depends on ACE2 and TMPRSS2 and Is Blocked by a Clinically Proven Protease Inhibitor. *Cell* **2020**, *181*, 271–280.e278. [CrossRef]
22. Wang, F.; Flanagan, J.; Su, N.; Wang, L.C.; Bui, S.; Nielson, A.; Wu, X.; Vo, H.T.; Ma, X.J.; Luo, Y. RNAscope: A novel in situ RNA analysis platform for formalin-fixed, paraffin-embedded tissues. *J. Mol. Diagn.* **2012**, *14*, 22–29. [CrossRef]
23. Klinkhammer, B.M.; Djudjaj, S.; Kunter, U.; Palsson, R.; Edvardsson, V.O.; Wiech, T.; Thorsteinsdottir, M.; Hardarson, S.; Foresto-Neto, O.; Mulay, S.R.; et al. Cellular and Molecular Mechanisms of Kidney Injury in 2,8-Dihydroxyadenine Nephropathy. *J. Am. Soc. Nephrol.* **2020**, *31*, 799–816. [CrossRef]
24. von Stillfried, S.; Villwock, S.; Bulow, R.D.; Djudjaj, S.; Buhl, E.M.; Maurer, A.; Ortiz-Bruchle, N.; Celec, P.; Klinkhammer, B.M.; Wong, D.W.L.; et al. SARS-CoV-2 RNA screening in routine pathology specimens. *Microb. Biotechnol.* **2021**. [CrossRef]
25. Remmelink, M.; De Mendonca, R.; D'Haene, N.; De Clercq, S.; Verocq, C.; Lebrun, L.; Lavis, P.; Racu, M.L.; Trepant, A.L.; Maris, C.; et al. Unspecific post-mortem findings despite multiorgan viral spread in COVID-19 patients. *Crit. Care* **2020**, *24*, 495. [CrossRef]
26. Sato, S.; Uejima, Y.; Arakawa, Y.; Furuichi, M.; Suganuma, E.; Fujinaga, S.; Nakazawa, A.; Kawano, Y. Clinical features of macrophage activation syndrome as the onset manifestation of juvenile systemic lupus erythematosus. *Rheumatol. Adv. Pract.* **2019**, *3*, rkz013. [CrossRef] [PubMed]
27. Bradley, B.T.; Maioli, H.; Johnston, R.; Chaudhry, I.; Fink, S.L.; Xu, H.; Najafian, B.; Deutsch, G.; Lacy, J.M.; Williams, T.; et al. Histopathology and ultrastructural findings of fatal COVID-19 infections in Washington State: A case series. *Lancet* **2020**, *396*, 320–332. [CrossRef]
28. Hopfer, H.; Herzig, M.C.; Gosert, R.; Menter, T.; Hench, J.; Tzankov, A.; Hirsch, H.H.; Miller, S.E. Hunting coronavirus by transmission electron microscopy—A guide to SARS-CoV-2-associated ultrastructural pathology in COVID-19 tissues. *Histopathology* **2021**, *78*, 358–370. [CrossRef]
29. Smith, K.D.; Akilesh, S.; Alpers, C.E.; Nicosia, R.F. Am I a coronavirus? *Kidney Int.* **2020**, *98*, 506–507. [CrossRef]
30. Polak, S.B.; Van Gool, I.C.; Cohen, D.; von der Thusen, J.H.; van Paassen, J. A systematic review of pathological findings in COVID-19: A pathophysiological timeline and possible mechanisms of disease progression. *Mod. Pathol.* **2020**, *33*, 2128–2138. [CrossRef]
31. Bosmuller, H.; Traxler, S.; Bitzer, M.; Haberle, H.; Raiser, W.; Nann, D.; Frauenfeld, L.; Vogelsberg, A.; Klingel, K.; Fend, F. The evolution of pulmonary pathology in fatal COVID-19 disease: An autopsy study with clinical correlation. *Virchows Arch.* **2020**, *477*, 349–357. [CrossRef]
32. Hwang, D.M.; Chamberlain, D.W.; Poutanen, S.M.; Low, D.E.; Asa, S.L.; Butany, J. Pulmonary pathology of severe acute respiratory syndrome in Toronto. *Mod. Pathol.* **2005**, *18*, 1–10. [CrossRef] [PubMed]
33. Nicholls, J.M.; Poon, L.L.; Lee, K.C.; Ng, W.F.; Lai, S.T.; Leung, C.Y.; Chu, C.M.; Hui, P.K.; Mak, K.L.; Lim, W.; et al. Lung pathology of fatal severe acute respiratory syndrome. *Lancet* **2003**, *361*, 1773–1778. [CrossRef]
34. Matschke, J.; Lutgehetmann, M.; Hagel, C.; Sperhake, J.P.; Schroder, A.S.; Edler, C.; Mushumba, H.; Fitzek, A.; Allweiss, L.; Dandri, M.; et al. Neuropathology of patients with COVID-19 in Germany: A post-mortem case series. *Lancet Neurol.* **2020**, *19*, 919–929. [CrossRef]
35. Ackermann, M.; Verleden, S.E.; Kuehnel, M.; Haverich, A.; Welte, T.; Laenger, F.; Vanstapel, A.; Werlein, C.; Stark, H.; Tzankov, A.; et al. Pulmonary Vascular Endothelialitis, Thrombosis, and Angiogenesis in Covid-19. *N. Engl. J. Med.* **2020**, *383*, 120–128. [CrossRef]
36. Buetti, N.; Patrier, J.; Le Hingrat, Q.; Loiodice, A.; Bouadma, L.; Visseaux, B.; Timsit, J.F. Risk factors for SARS-CoV-2 detection in blood of critically ill patients. *Clin. Infect. Dis.* **2020**. [CrossRef]
37. Tan, S.H.; Allicock, O.; Armstrong-Hough, M.; Wyllie, A.L. Saliva as a gold-standard sample for SARS-CoV-2 detection. *Lancet Respir. Med.* **2021**, *9*, 562–564. [CrossRef]

38. Huang, N.; Perez, P.; Kato, T.; Mikami, Y.; Okuda, K.; Gilmore, R.C.; Conde, C.D.; Gasmi, B.; Stein, S.; Beach, M.; et al. SARS-CoV-2 infection of the oral cavity and saliva. *Nat. Med.* **2021**. [CrossRef]
39. Puelles, V.G.; Lutgehetmann, M.; Lindenmeyer, M.T.; Sperhake, J.P.; Wong, M.N.; Allweiss, L.; Chilla, S.; Heinemann, A.; Wanner, N.; Liu, S.; et al. Multiorgan and Renal Tropism of SARS-CoV-2. *N. Engl. J. Med.* **2020**, *383*, 590–592. [CrossRef]
40. Sekulic, M.; Harper, H.; Nezami, B.G.; Shen, D.L.; Sekulic, S.P.; Koeth, A.T.; Harding, C.V.; Gilmore, H.; Sadri, N. Molecular Detection of SARS-CoV-2 Infection in FFPE Samples and Histopathologic Findings in Fatal SARS-CoV-2 Cases. *Am. J. Clin. Pathol.* **2020**, *154*, 190–200. [CrossRef]
41. Li, D.; Jin, M.; Bao, P.; Zhao, W.; Zhang, S. Clinical Characteristics and Results of Semen Tests Among Men With Coronavirus Disease 2019. *JAMA Netw. Open* **2020**, *3*, e208292. [CrossRef]
42. Yang, M.; Chen, S.; Huang, B.; Zhong, J.M.; Su, H.; Chen, Y.J.; Cao, Q.; Ma, L.; He, J.; Li, X.F.; et al. Pathological Findings in the Testes of COVID-19 Patients: Clinical Implications. *Eur. Urol. Focus* **2020**, *6*, 1124–1129. [CrossRef]
43. Hanley, B.; Naresh, K.N.; Roufosse, C.; Nicholson, A.G.; Weir, J.; Cooke, G.S.; Thursz, M.; Manousou, P.; Corbett, R.; Goldin, R.; et al. Histopathological findings and viral tropism in UK patients with severe fatal COVID-19: A post-mortem study. *Lancet Microbe* **2020**, *1*, e245–e253. [CrossRef]
44. Wichmann, D.; Sperhake, J.P.; Lutgehetmann, M.; Steurer, S.; Edler, C.; Heinemann, A.; Heinrich, F.; Mushumba, H.; Kniep, I.; Schroder, A.S.; et al. Autopsy Findings and Venous Thromboembolism in Patients With COVID-19: A Prospective Cohort Study. *Ann. Intern. Med.* **2020**, *173*, 268–277. [CrossRef]
45. Wei, L.; Sun, S.; Xu, C.H.; Zhang, J.; Xu, Y.; Zhu, H.; Peh, S.C.; Korteweg, C.; McNutt, M.A.; Gu, J. Pathology of the thyroid in severe acute respiratory syndrome. *Hum. Pathol.* **2007**, *38*, 95–102. [CrossRef]
46. Guerini-Rocco, E.; Taormina, S.V.; Vacirca, D.; Ranghiero, A.; Rappa, A.; Fumagalli, C.; Maffini, F.; Rampinelli, C.; Galetta, D.; Tagliabue, M.; et al. SARS-CoV-2 detection in formalin-fixed paraffin-embedded tissue specimens from surgical resection of tongue squamous cell carcinoma. *J. Clin. Pathol.* **2020**, *73*, 754–757. [CrossRef]
47. van Dam, P.A.; Huizing, M.; Mestach, G.; Dierckxsens, S.; Tjalma, W.; Trinh, X.B.; Papadimitriou, K.; Altintas, S.; Vermorken, J.; Vulsteke, C.; et al. SARS-CoV-2 and cancer: Are they really partners in crime? *Cancer Treat. Rev.* **2020**, *89*, 102068. [CrossRef] [PubMed]
48. Sungnak, W.; Huang, N.; Becavin, C.; Berg, M.; Queen, R.; Litvinukova, M.; Talavera-Lopez, C.; Maatz, H.; Reichart, D.; Sampaziotis, F.; et al. SARS-CoV-2 entry factors are highly expressed in nasal epithelial cells together with innate immune genes. *Nat. Med.* **2020**, *26*, 681–687. [CrossRef]
49. Kusmartseva, I.; Wu, W.; Syed, F.; Van Der Heide, V.; Jorgensen, M.; Joseph, P.; Tang, X.; Candelario-Jalil, E.; Yang, C.; Nick, H.; et al. Expression of SARS-CoV-2 Entry Factors in the Pancreas of Normal Organ Donors and Individuals with COVID-19. *Cell Metab.* **2020**, *32*, 1041–1051. [CrossRef]
50. Song, J.; Li, Y.; Huang, X.; Chen, Z.; Li, Y.; Liu, C.; Chen, Z.; Duan, X. Systematic analysis of ACE2 and TMPRSS2 expression in salivary glands reveals underlying transmission mechanism caused by SARS-CoV-2. *J. Med. Virol.* **2020**, *92*, 2556–2566. [CrossRef]
51. Song, H.; Seddighzadeh, B.; Cooperberg, M.R.; Huang, F.W. Expression of ACE2, the SARS-CoV-2 receptor, and TMPRSS2 in prostate epithelial cells. *bioRxiv* **2020**. [CrossRef]
52. Cantuti-Castelvetri, L.; Ojha, R.; Pedro, L.D.; Djannatian, M.; Franz, J.; Kuivanen, S.; van der Meer, F.; Kallio, K.; Kaya, T.; Anastasina, M.; et al. Neuropilin-1 facilitates SARS-CoV-2 cell entry and infectivity. *Science* **2020**, *370*, 856–860. [CrossRef]
53. Speranza, E.; Williamson, B.N.; Feldmann, F.; Sturdevant, G.L.; Perez-Perez, L.; Meade-White, K.; Smith, B.J.; Lovaglio, J.; Martens, C.; Munster, V.J.; et al. Single-cell RNA sequencing reveals SARS-CoV-2 infection dynamics in lungs of African green monkeys. *Sci. Transl. Med.* **2021**, *13*, 578. [CrossRef]
54. Grant, R.A.; Morales-Nebreda, L.; Markov, N.S.; Swaminathan, S.; Querrey, M.; Guzman, E.R.; Abbott, D.A.; Donnelly, H.K.; Donayre, A.; Goldberg, I.A.; et al. Circuits between infected macrophages and T cells in SARS-CoV-2 pneumonia. *Nature* **2021**, *590*, 635–641. [CrossRef]
55. Zhao, Y.; Zhao, Z.; Wang, Y.; Zhou, Y.; Ma, Y.; Zuo, W. Single-Cell RNA Expression Profiling of ACE2, the Receptor of SARS-CoV-2. *Am. J. Respir. Crit. Care Med.* **2020**, *202*, 756–759. [CrossRef]